



Investigation of heat-spreaders as a passive thermal management element in SWIR fiber lasers

HELENA PICMAUSOVÁ,^{1,2,*}  MICHAEL PÍSAŘÍK,¹
CLÉMENT ROMANO,¹  DIETER PANITZEK,^{1,3} JAN FARLÍK,²
MARC EICHHORN,^{1,3} AND CHRISTELLE KIELECK¹

¹Fraunhofer IOSB (Institute of Optronics, System Technologies and Image Exploitation), Gutleuthausstraße 1, 76275, Ettlingen, Germany

²University of Defence, Kounicova 65, 66210, Brno, Czech Republic

³Institute of Control Systems (IRS), Karlsruhe Institute of Technology (KIT), Fritz-Haber-Weg 1, 76131, Karlsruhe, Germany

*helena.picmausova@iosb.fraunhofer.de

Abstract: This article examines the utility of heat spreaders as an alternative to conventional heat management techniques for fiber lasers and amplifiers by numerical modeling scalable for prediction of heat loads in high power laser amplifiers and the model's experimental verification. A special focus is placed on the section of a fiber splice, given its importance and potential issues associated with signal loss and subsequent heat generation during laser operation. Temperature change is analyzed and compared both numerically and experimentally for three passive cooling architectures: a loose, recoated fiber splice attached to a copper plate via Kapton tape, a recoated fiber splice placed in a thermal interface material (TIM) filled U-shaped groove in an aluminum plate, and finally a non-recoated splice placed in a heat-spreader, with the recoating material serving instead of TIM. The benefits and utility of fiber heat spreaders are shown and discussed, and their superior thermal transfer rate is demonstrated.

© 2025 Optica Publishing Group under the terms of the [Optica Open Access Publishing Agreement](#)

1. Introduction

Efficient heat management is one of the key challenges for fiber laser and amplifier design and operation. Fiber lasers operating in the SWIR (short-wave infrared) region have been pushed to ever-higher levels of performance due to large gain length with high confinement of the propagating mode, resulting in high output power and exceptional beam quality. These systems offer a unique combination of attributes that make them a highly desirable solution when aiming for size, weight, and power (SWaP) consumption optimization. Fibers can be coiled, making the laser much less bulky than free space optical systems, and intrinsically offer a high surface area to volume ratio for better heat dissipation. Furthermore, optimized silica fibers offer excellent transparency [1] even up to 2 μm and beyond.

Even so, heat generation in a fiber laser still occurs in the form of an intrinsic or an extrinsic loss. The former includes nonradiative relaxation processes and quantum defect of the gain elements. The latter is associated with optical loss at fiber joints and intrinsic absorption including the presence of light-absorbing impurities such as Fe, Cu, or OH, which may be reduced through careful control of fiber manufacturing [2,3].

While elastic scattering such as Rayleigh scattering does not produce heat directly, it can subsequently be absorbed within the fiber [1,4]. Inelastic scattering such as Stimulated Raman Scattering (SRS) and Stimulated Brillouin Scattering (SBS) also have a quantum defect and therefore generate heat. However, quantum defect induced heat is only important when building fiber lasers that use these processes intentionally for wavelength conversion [5].

Adverse effects of heat in fiber lasers and amplifiers vary in severity, and include (but are not limited to): change of absorption and emission cross-sections, degradation of fiber coating polymers, and thermal non-linearities such as transverse mode instability (TMI) and thermal lensing, and phase and intensity noise [2].

Additionally, excessive heat generation can lead to additional thermal induced mechanical stress. Fiber coatings generally have a maximum handling temperature threshold at around 85°C as a standard, and up to 125°C for specialty coatings, setting a limiting point for laser operation. The importance of sustainable power extraction cannot therefore be overstated, not only for high-power applications, but also in lower-power, high-precision laser sensing systems [2,6]. Heat spreaders are widely used in semiconductor industry [7] and in high power lasers such as thin-disc lasers [8] or Ti:Sapph [9]. The main idea of this technology is the utilization of a high thermal conductivity material like diamond or SiC and thermally connect it using adielectric material to a dedicated heating zone - this distributes the heat load into a bigger area. Thickness of the connecting dielectric material should be $< 10 \mu\text{m}$ to get the most benefits from this technology.

2. Heat management options – similar and alternative technologies

Heat management generally involves a form of either active or passive cooling. While passive cooling relies on natural thermal conduction or convection due to the temperature gradient between e.g. a heat sink and the heat source, active cooling solutions such as a Peltier device consume additional energy to operate. Both solutions usually add additional volume and weight to the system, which is in conflict with the low SWaP potential of fiber architectures and can induce added mechanical stress or vibrations and consequently influence refractive index through photoelastic effect. Additionally, any asymmetry in cooling creates additional temperature gradients which can result in mode distortion [4–6].

Furthermore, material engineering of fiber glass has led to purely optical cooling methods that have been explored in [1–3]. Detailed temperature investigation of a double-clad Tm^{3+} -doped fiber MOPA system for high-power operation has been presented in [10], with the recoated splice clearly identified as the hottest fiber region. The focus of this paper, therefore, is to offer an improved approach to thermal management of a recoated fiber splice using heat spreader technology presented below; with the goal of bringing the thermal load on the splice below the levels of thermal load observed in the rest of the fiber and subsequently improving overall performance of the system.

3. Heat spreader architecture and properties

In this study, a 125 μm diameter fiber splice is recoated with a layer of polymer, adding a layer of 72.5 μm , totaling 270 μm in diameter. This relatively thick layer of the polymer plays a detrimental role due to its low thermal conductivity as listed in Table 1, relative to other presented materials.

Table 1. Thermal properties of used materials

Material	Fiber glass	Polymer coating	TiM	Copper	Aluminum	SiC
Thermal conductivity coefficient [$\text{W} \cdot \text{m}^{-1} \cdot \text{K}^{-1}$]	1.38	0.18	3	400	201	490
Thermal expansion coefficient [$10^{-6} \cdot \text{K}^{-1}$]	0.51	50	70	17	23	3.5
Heat capacity at constant pressure [$\text{J}/(\text{kg} \cdot \text{K})$]	772	1470	470	385	900	750

Overview of all architectures investigated in this paper is presented in Fig. 1, heat spreaders, as described in the schematic c) in Fig. 1, offer some inherent advantages due to their architecture, and used materials' structural and thermal properties, which are explained below:

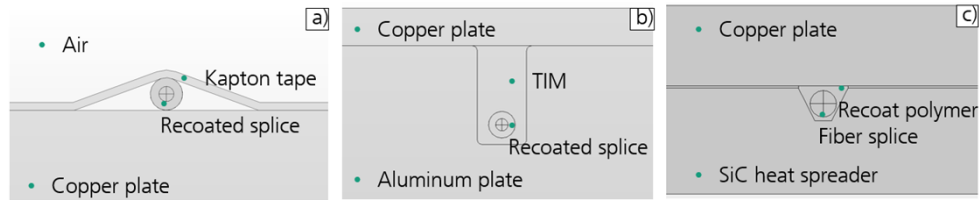


Fig. 1. Schematics of investigated architectures: a) a recoated splice taped to a copper plate, b) a recoated splice placed in an aluminum groove with thermal interface material (TIM), and c) a splice recoated directly in a heat spreader.

When dealing with a recoated fiber taped to a cold plate, as presented in Fig. 1(a), difficulties arise due to low thermal conductivity of the recoating polymer, and insufficient thermal contact with the cold plate. This architecture is also challenging for numerical methods, as it is difficult to accurately model thermal contact between the recoated fiber and the plate, even when accounting for thermal expansion of materials.

Variously shaped grooves machined in metal plates as seen in Fig. 1(b) pose additional challenges. Generally, when dealing with metal plates, U-shaped grooves offer an advantage from a heat management point of view, and mechanically easier insertion of the fiber than V-shaped grooves, however they are also more difficult to machine, especially for small diameter fibers.

While the groove is usually filled with a highly conductive thermal grease or other TIM, the issues of the polymer recoat thickness and low thermal conductivity remains. Additionally, aluminum and other metals possess a much higher thermal expansion coefficient than fiber glass, also listed in Table 1, which adds mechanical stress and can lead to damage of the splice, despite the recoating polymer's elasticity [11]. Often, delamination will occur between the fiber and its coating or recoating, leading to degradation of the pump propagation, and consequently of the optical performance, creation of a hot spot, which can lead to permanent damage to the laser [12].

Compared to these, the heat-spreader architecture (Fig. 1(c)) offers inherent advantage when dealing with splice heat management. The heat spreader silicon carbide (SiC) plate, into which a V-shaped groove is machined, has comparable thermal expansion value to fiber glass, therefore doesn't add mechanical stress on the splice when heated, and has excellent thermal conductivity properties. Additionally, very precise machining of the V-groove is possible, allowing for the spliced fiber to be placed directly in the groove, which is then filled with the recoating polymer. The resulting layer of polymer is much thinner than the recoating layer of a splice, going as low as $10\ \mu\text{m}$ and allowing for more efficient heat transfer from the fiber.

4. Numerical models

In most fiber laser systems, the splices between fibers generally require increased attention and careful handling, as they are one of the critical points for thermal and mechanical stress management. Therefore, a spliced segment of a fiber laser was chosen to be investigated in detail. Total heating power in all versions of the numerical model was set to an estimated $50\ \text{mW/cm}$, which corresponds to approximately $5\ \text{W}$ of pump power in the following experiment and is represented as a linear heat source with a radius of $1\ \mu\text{m}$, co-axial with the fiber core to mimic quantum defect induced heating. The ambient temperature is set at $293.15\ \text{K}$.

The temperature gradient and the effective thermal conductivity are used to evaluate the conductive heat flux within the model using finite element analysis (FEA). The heat conduction

is solved for using Fourier's law for continuous media. Surface-to-ambient radiation is also considered, as well as external free convection off the plate surface.

Key thermal properties of materials used in the model, including the thermal interface material (TIM) are in Table 1. Values were obtained via communication with various suppliers, for the polymer recoating as reported in [10].

Three different heat management solutions of the splice were considered:

1. Active-to-passive fiber splice, recoated to a diameter of $270\ \mu\text{m}$, secured to an actively cooled copper plate using a Kapton film tape. Results of the numerical model are presented in Fig. 2. A slight heat expansion is considered in the model, resulting in a homogenous thermal contact between the fiber and the plate. This thermal contact is expected to be lower in real, experimental setting.

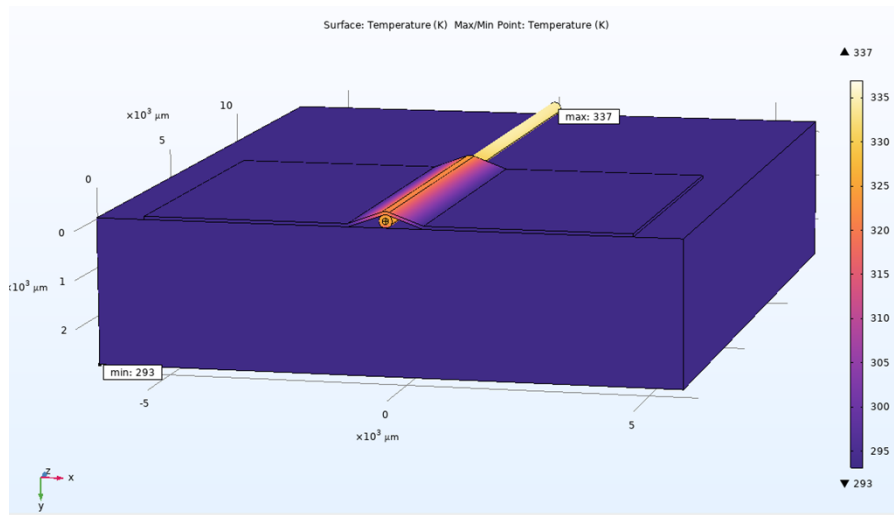


Fig. 2. Numerical model of heat distribution within the first configuration: A fiber splice is recoated to $270\ \mu\text{m}$ in diameter and attached to a copper cold-plate using Kapton tape.

2. Identical fiber splice is inserted in a U-shaped groove machined in an aluminum block. The groove is filled with thermal paste and subsequently covered with a copper lid. The numerical model of the setup is rendered in Fig. 3, semi-transparent for better clarity.
3. Fiber splice with no polymer recoating is placed into a heat-spreader. The heat-spreader consists of a block of silicon carbide (SiC) with a machined V – groove, and a copper lid. The recoating polymer is poured directly into the V – groove and forms a thin layer between the SiC block and the copper lid, as seen in Fig. 4.

Results for each model with rendered isothermal contours are presented in Figs. 5–7.

Each of the 3D models have the point of maximum temperature highlighted. With identical heat load of $50\ \text{mW/cm}$, the first architecture with Kapton tape exhibits the highest maximum temperature of $337\ \text{K}$. Thermal expansion of materials is considered, used values of TEC are listed in Table 1. The aluminum U-groove setup and the heat spreader architecture offer similar results regarding heat load, the former exhibiting a maximum of $299\ \text{K}$, the latter of $297\ \text{K}$.

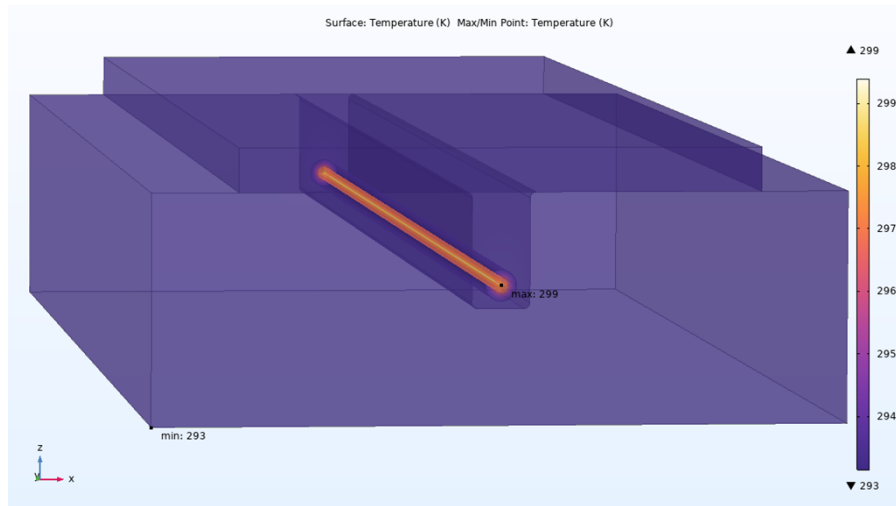


Fig. 3. Numerical model of heat distribution within the second configuration: A fiber splice, recoated to 270 μm , is placed in a U-groove in an aluminum block, with the groove filled with thermal paste and covered with a copper lid. For greater clarity, the model is rendered transparent.

5. Experimental setup and results

A schematic overview of the experimental setup is presented in Fig. 8. An optical backscatter reflectometer (OBR) was used to measure the temperature change inside the passive/active fiber core. Aside from the advantage of acquiring data directly from the fiber core [13], the OBR was selected for future measurements of a complete Er-Yb co-doped fiber laser system or ASE source. Er-Yb co-doped fiber has lower quantum efficiency and higher bleaching threshold level than Yb doped fiber and has no emission or absorption around 1.3 μm wavelength, important for the OBR measurement spectral window between 1270 to 1350 nm.

For the experimental evaluation, a 2 m long EY1 active fiber was selected, acting as an amplified spontaneous emission (ASE) source. An ASE source has a higher temperature load of the active fiber, and it should provide better resolution in relative measurement for comparison of different fiber heat management methods. Using technical specifications of the fiber, and assuming the pump wavelength of 976 nm, the total linear heat density of the fiber was calculated at 26 ± 5 mW/cm per W of pump power. Real pump absorption was not the focus of this investigation, but rather a robust comparison of different thermal management options. To reduce spontaneous emission of Yb ions at around 1 μm wavelength towards the OBR, a counter-pumped scheme was used, as the forward ASE was exhibiting approximately 30 times lower power values than the backward ASE. The passive 1550 nm double clad fiber resp. EY1 fiber single mode (SM) cut off is reported by the manufacturer at 1440 nm, resp. 1470 nm.

The multimode regime of EY1 and the passive fiber could affect the OBR measurement and could generate echo spikes or artefacts after high stress events [13]; therefore, the fiber structure was fixed onto an aluminum plate by Kapton tape for stabilization of multimodal propagation to achieve comparable measurement conditions, as referenced in Fig. 9. A water-cooled copper block was also used in the area of interest, focusing on the most loaded passive to active fiber splice and an approx. 100 mm zone around it. Thermal grease was used to provide better thermal contact, especially in areas of active fiber elevation on interfaces such as aluminum plate to copper block, recoating of fiber and heat spreader. A reflective wavelength-division multiplexer (WDM) with additional filter was used to block ASE at 1 μm from Yb ions to protect the OBR

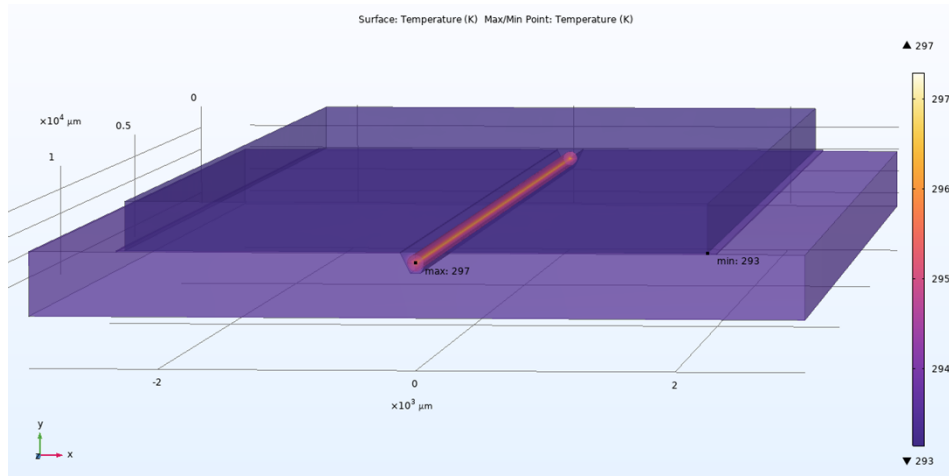


Fig. 4. Numerical model of heat distribution within the third configuration: A fiber splice with no recoating is placed in a V-groove in an SiC heat-spreader, recoating polymer is used to fill the groove and forms a thin layer between the heat-spreader and a copper lid. For greater clarity, the model is rendered transparent.

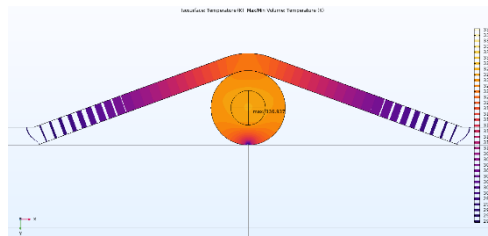


Fig. 5. Detail of isothermal contours within the first configuration: a recoated splice attached to a copper cold-plate using Kapton tape. Maximum simulated temperature 337 K.

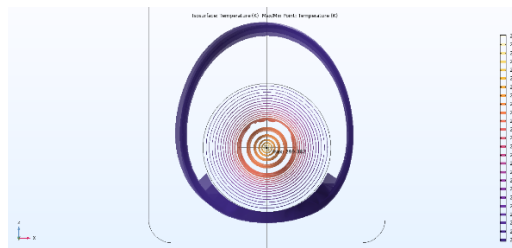


Fig. 6. Detail of isothermal contours for the second configuration: a recoated splice placed in a U-groove within an aluminum block. Maximum simulated temperature 299 K.

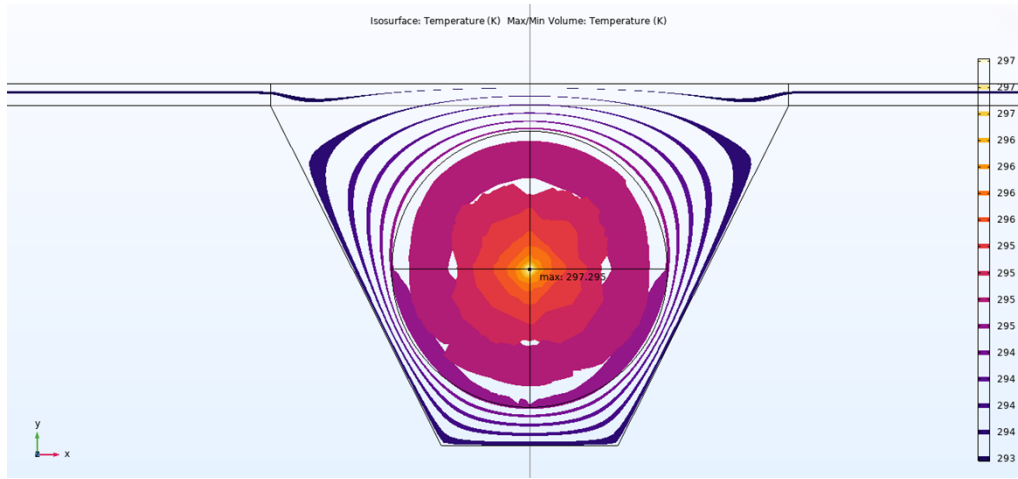


Fig. 7. Detail of isothermal contours distribution in the third configuration: A fiber splice with no recoating is placed in an SiC heat-spreader. Maximum simulated temperature 297 K.

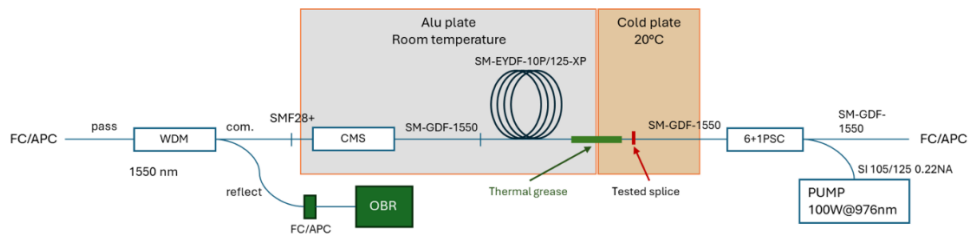


Fig. 8. Schematic of the experimental setup. CMS: cladding mode stripper, WDM: reflective type cold mirror wavelength-division multiplexer.

detector. The limiting condition of the experiment was determined at 1 mW safety threshold of ASE power at the OBR detector. A maximum of 200 μ W of forward ASE power at 5 W of pump power was measured.

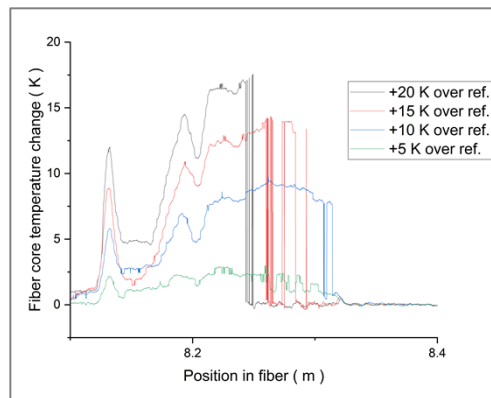


Fig. 9. Echoes in passive LMA fiber placed on cold plate from fiber termination 20 cm from measuring point. Reference was taken at 293 K.

Three different fiber heat management architectures were investigated for comparison with the numerical model. First, a recoated splice at 270 μm total diameter, attached to a cold plate with Kapton tape. Second, a recoated splice was inserted into a 40 mm long aluminum block with a U shape groove approximately 550 μm wide and 1 mm deep. Finally, a splice of active and passive fiber was inserted directly without a recoat into 20 mm long SiC heat spreader, with 2 mm separation length and a point contact to the cold plate.

Measurement errors were minimized by averaging over a 10 mm distance of the fiber, comparing different techniques of splice management. Two points of interest were marked as indicated by the vertical lines in Fig. 10: one directly on the active fiber on Al plate to compare with the pump power value, and a second one directly at the splice between the active and passive fiber. Reference measurement was taken before each measurement after thermal stabilization. Evolution of temperature inside the active fiber in Fig. 10 was not smooth due to variations in thermal contact of the active fiber and the Al plate taped down with Kapton at approximately 90°.

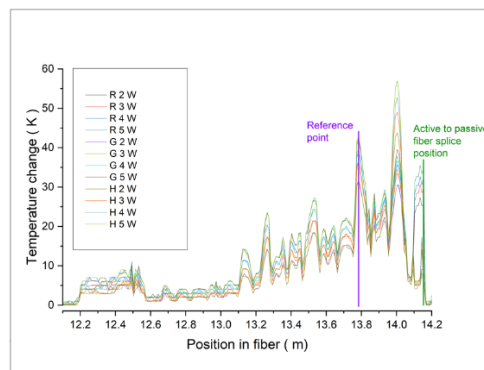


Fig. 10. Temperature change from the ambient temperature in active and passive fiber for different thermal management methods and pump power from 2 W to 5 W, R is fiber splice recoated by polymer and taped by Kapton tape to cold plate, G is fiber splice recoated by polymer and placed in U-groove inside Al cold plate, H is fiber splice recoated by polymer directly in SiC heat spreader.

Difference in length of the aluminum U-groove and the heat spreader is indicated in close detail in Fig. 11, which shows the temperature change measurement of the splice region for the aluminum plate and heat spreader architectures in comparison.

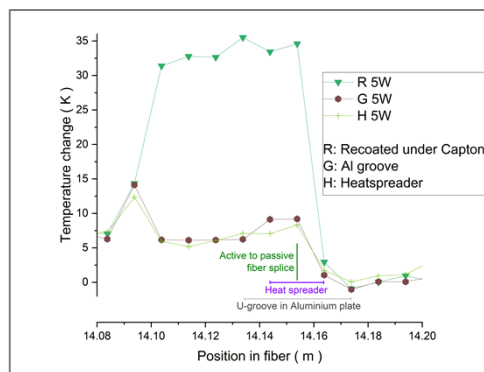


Fig. 11. Detail of temperature change measurement in the splice region, with indication of the heat spreader and aluminum plate sizes at 5 W of pump power.

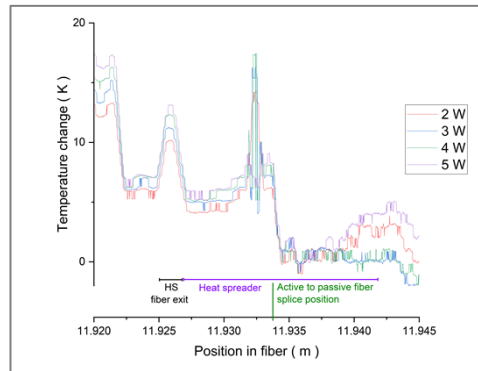


Fig. 12. Temperature change measured with $20\ \mu\text{m}$ resolution without averaging of active to passive splice region inside SiC heat spreader in relation to pump power.

When increasing the pump power from 3 W to 5 W, experimental measurements in the heat spreader showed a measurement artefact, by not corresponding change of temperature to pump power. The measurement artefacts, as seen in Fig. 12, were likely caused by a change in stress in the fiber because measured temperature change decreased with increase of pump power. Another measurement was taken with $20\ \mu\text{m}$ step resolution without averaging over the fiber length [13]. Also, one of the cold mirror filters was removed to increase OBR resolution by widening the spectral window. The reference start position inside the fiber was changed by approximately 2 m.

High resolution measurement of temperature change inside the heat spreader in Fig. 12 is exhibiting non-linear dependency on pump power and random behavior at 4 W and 5 W pump power in both directions from active to passive fiber splice (artefact) indicating mechanical stress change. This stress could be caused by microbubble formation inside the low index polymer or by micro-bending due to a dust particle. Excluding this error by removing part of measurement artefact data, the temperature change inside the heat spreader was measured at 5.8 K for 5 W of pump power.

Comparison of temperature change values obtained from the numerical models and experimental measurements for each configuration is presented in the table in Table 2. The reference point indicated in the graphs and the table served as a benchmark for the experiment, to ascertain that no loss caused by contamination of the splice occurs and that full pump power reaches the examined splice.

Table 2. Temperature change values obtained from experimental measurements and the numerical models

	<i>Experiment - Reference point</i>				<i>Experiment - Splice location</i>				<i>Numerical model</i>
<i>Position</i>	13.784				14.154				-
<i>Pump power (W)</i>	2	3	4	5	2	3	4	5	5
<i>Recoated splice (K)</i>	31.59	36.50	38.69	41.89	25.47	29.52	32.44	34.59	42.85
<i>Recoated splice inside Al-groove (K)</i>	31.38	34.79	38.63	41.91	7.10	7.34	8.31	9.20	5.85
<i>Splice inside heat spreader (K)</i>	31.59	36.54	39.69	42.73	6.23	7.11	8.14	8.23	3.85
<i>Splice inside heat Spreader in high resolution (K)</i>	-	-	-	-	4.33	5.04	5.50	5.80	3.85

Both numerical model and experimental measurement indicate improved thermal transfer rate in the heat spreader architecture, and a decrease in temperature change in the fiber splice. The

temperature change in the heat spreader is shown to stay below the value of temperature change in the active optical fiber section, making the properties of the active fiber the limiting factor for thermal management, rather than the splice itself.

Additionally, temperature sensitivity to increased levels of dust contamination was documented throughout the experiment, mostly resulting from manipulation of the fiber without its polymer coating.

6. Discussion and conclusion

Throughout this work, heat spreaders were investigated as an important method of passive thermal management architecture for fiber lasers. The focus was on the region surrounding an active to passive fiber splice, as splices represent a critical point for thermal and mechanical stress management in fiber laser systems. Three different approaches were compared both experimentally and numerically: A recoated splice placed on a water-cooled copper block and secured by Kapton tape, a recoated splice placed in a U-shaped groove in an aluminum block, and a splice with a recoat layer of polymer directly inside a heat spreader.

For the simple recoated fiber taped to a cooled plate approach, a higher value of the temperature change was predicted in the numerical model than the value measured experimentally. This is likely due to a smaller area of thermal contact predicted in the model compared to the experiment, as thermal properties of the soft recoating polymer are often insufficiently defined for optical fibers. Other cause of discrepancy between the numerical model and the experimental data is likely caused by inherent splice loss. Even so, the model and the experimental data correlate very closely.

Temperature change measured and modelled within the heat spreader architecture during operation is below the values measured throughout the regular section of the active fiber, making the fiber itself the limiting factor for heat management, not the cooled splice area.

Heat spreader architecture was demonstrated as promising compared to other fiber thermal management methods for multiple reasons, including the possibility of significantly reducing polymer recoating thickness. This resulted in a reduction of fiber splice temperature below the value measured in the originally coated active fiber and lessened thermal-induced stress load on the splice due to similar thermal expansion coefficient to that of fiber glass, corresponding to the temperature change from the fiber core to coolant.

Obtained experimental data was proven highly accurate even during mildly multimode operation, and a small temperature change generated a microbubble in the recoating polymer was documented. Splice and recoat quality were thoroughly evaluated.

Funding. Ministerstvo Obrany České Republiky Czech Republic Ministry of Defence; University of Defence Development Program (DZRO - Conduct of Airspace Operations); German Federal Ministry Of Defence.

Acknowledgment. We'd like to thank the mechanical workshop of the IOSB and Artur Schander, who fabricated opto-mechanical components for the experimental setup.

Disclosures. The authors declare no conflict of interest.

Data availability. Data underlying the results presented in this paper is not publicly available at this time but may be obtained from the authors upon reasonable request.

References

1. J. Ballato and P. D. Dragic, "The uniqueness of glass for passive thermal management for optical fibers," *Int J Appl Glass Sci* **13**(3), 267–280 (2022).
2. J. Ballato, P. D. Dragic, and M. Digonnet, "Prospects and challenges for all-optical thermal management of fiber lasers," *J. Phys. D: Appl. Phys.* **57**(16), 162001 (2024).
3. J. F. Michel, John Digonnet, Peter D. Ballato, *et al.*, "Anti-Stokes cooling and other thermal managements techniques in fiber lasers and amplifiers," *Proc. SPIE* 11981, Fiber Lasers XIX: Technology and Systems, 119810H (2022).
4. D. Panitzek, C. Romano, M. Eichhorn, *et al.*, "Temperature investigation of low SWaP thulium-doped fiber lasers," *Opt. Express* **32**(2), 1890–1901 (2024).

5. D. Panitzek, C. Romano, M. Písařík, *et al.*, “Temperature and pump modulation investigation of an Er:Yb co-doped fiber laser with optimized SWaP,” *Opt. Express* **33**(3), 3851–3860 (2025).
6. Marc-André Lapointe, Stéphane Chatigny, Michel Piché, *et al.*, “Thermal effects in high-power CW fiber lasers,” *Proc. SPIE* 7195, Fiber Lasers VI: Technology, Systems, and Applications, 71951U (19 February 2009).
7. Zhen Yan, Wenyi Tong, Xiangyu Wang, *et al.*, “A review of diamond composites for heat spreaders, Composites Part A”: Applied Science and Manufacturing, 196, 109008 (2025).
8. C. J. Saraceno, D. Sutter, T. Metzger, *et al.*, “The amazing progress of high-power ultrafast thin-disk lasers,” *J. Eur. Opt. Soc.-Rapid Publ.* **15**, 1 (2019).
9. J. Hinnerk Wolter, R. Balmer, M. Antier, *et al.*, “Ti:sapphire thin-disk laser symmetrically cooled by curved single crystal diamond heat spreaders,” *2020 Laser Phys. Lett* **17**, 015802 (2019).
10. Till Walbaum, Matthias Heinzig, Franz Beier, *et al.*, “Spatially resolved measurement of the core temperature in a high-power thulium fiber system,” *Proc. of SPIE* Vol. 9728, 97280P, Fiber Lasers XIII: Technology, Systems, and Applications, (2016).
11. Tao Chen, Shangzhi Song, Yang Shen, *et al.*, “Simultaneous measurement of thermal conductivity and heat capacity across diverse materials using the square-pulsed source (SPS) technique,” *International Communications in Heat and Mass Transfer* **158**, 107849 (2024).
12. B. Topper, S. Kuhn, A. Neumann, *et al.*, “Laser cooling ytterbium doped silica by 67 K from ambient temperature,” *Opt. Express* **32**(3), 3660–3672 (2024).
13. LUNA Innovations Incorporated, “Distributed fiber optic sensing: temperature compensation of strain measurement,” Engineering Note EN-FY1402 (2016).